

Influence of particle size distribution width on GFA index of uniaxially compressed granular materials

Ragunanth Venkatesh^a, Miha Brojan^a, Igor Emri^a, Arkady Voloshin^b, Edvard Govekar^{a,*}

^a Faculty of Mechanical Engineering, University of Ljubljana, Aškerčeva cesta 6, 1000 Ljubljana, Slovenia

^b Department of Mechanical Engineering and Mechanics, Lehigh University, 19 Memorial Drive West, Bethlehem, PA 18015, USA

ARTICLE INFO

Article history:

Received 15 May 2020

Received in revised form 21 August 2020

Accepted 13 September 2020

Available online 17 September 2020

Keywords:

Particle size distribution width

Uniaxial compression

GFA index

Internal friction

Flowability

Internal pressure ratio

ABSTRACT

This study investigates the influence of particle size distribution (PSD) width on the internal friction and internal pressure ratio of granular materials, and the related flowability of such material when uniaxially compressed in a closed volume. For this purpose, an optical granular friction analyzer (O-GFA) was used to evaluate the granular friction analyzer (GFA) index, which may be related to the internal friction and internal pressure ratio. By examining bronze powder samples with 3 different PSD widths it was shown that as PSD width increases, the load independent GFA index increases, internal friction decreases and the internal pressure ratio remains constant. Furthermore, our study confirms that, determining the GFA index using the O-GFA for characterizing the flowability of uniaxially compressed granular material is an alternative to traditional methods, which require the individual properties of granular materials i.e. internal friction and internal pressure ratio to be determined through two separate tests.

© 2020 Elsevier B.V. All rights reserved.

1. Introduction

Granular materials play an important role in numerous industries, including manufacturing, construction, pharmaceuticals, the automotive industry, powder metallurgy, paint-making, and agriculture, and are of interest in various scientific fields including physics, chemistry, mechanics, and engineering [1–3]. In industry, granular materials undergo various technological processes such as storing, compressing, mixing, filling and transporting, all of which are affected by the properties and behavior of the granular material. In addition to their mechanical response [4], one of the most important properties of granular materials is flowability, defined as the ability of particles to flow [5].

In general, the flowability of granular materials depends on their properties and the conditions under which flow and technological processing take place [5]. The main characteristics which influence the flowability of a given granular material are the geometric parameters of the particles, surface roughness, particle size distribution (PSD) and material properties, which include the chemical composition of the particles, stiffness and density.

With regard to the analysis of the influence of granular material properties and the associated flowability, studies reported in the literature have mainly focused on monodisperse granular materials [6]. Most

granular materials used in industry, however, consist of particles in a wide range of sizes, and an associated PSD [6]. PSD affects the properties of the granular materials, including the rearrangement of the particles and their contact network, resulting in different compaction properties, internal friction and flowability, which is important in any industry involving technological processing. Understanding the relationship between PSD and flowability is therefore important for industries where granular materials are processed.

Many different methods and types of test apparatus can be used to investigate the influence of PSD on the flowability of granular material [7]. Xinde et al. [7] studied the influence of PSD width on the flowability of β -carotene powders using the Hausner ratio [8], the flow index (Jenike shear test) [9], the angle of repose [10] and the bin-flow test [7]. Kurz et al. [11] used the Jenike shear apparatus [9] to investigate the same using limestone powders. Xinde et al. remarked that materials would exhibit good flowability when they contain a smaller amount of fine particles within larger particles, due to the “lubricating” ability of the smaller particles. Too many smaller particles, however, would increase the contact area (due to an increased surface to volume ratio), and thus decrease the flowability. Both Xinde et al. and Kurz et al. concluded that a wider PSD would lead to lower flowability. Luana et al. [12] investigated the influence of PSD on the flowability of coarse and fine sugar powders, using the Hausner ratio and repose angle method. Their results show that a wide PSD leads to a higher flowability compared to a narrow PSD, which is in direct contradiction to the results of Xinde et al. [7] and Kurz et al. [11]. This could either be due to the

Abbreviation: PSD, particle size distribution; GFA, granular friction analyzer.

* Corresponding author.

E-mail address: edvard.govekar@fs.uni-lj.si (E. Govekar).

material and geometric characteristics of the sugar powders used, or to the interrelation between the PSD mean and the width (both of which were varied).

In the cases mentioned above, the influence of the PSD of a granular material on its flowability was investigated without considering the conditions of technological processing. The flowability of a powder, however is not only influenced by the PSD and physical properties of the granular material, but also by the conditions under which flow and technological processing take place. In order to characterize flowability it is therefore important to perform experiments that replicate real applications as far as possible. An example, common to various powder industries, is the storage and conveyance of powder from a large silo, where granular materials are subjected to high compression due to gravity and the additional compressive force exerted to assist the flow of particles from the silo [5,13]. Such an example was considered by Wicke et al. [14], who used 3D discrete element modeling simulations to analyze the effect of the PSD shape on stress-strain and pressure transmission in granular materials under compression. Their findings show that the shape of the PSD affects the pressure transmission in granular materials, resulting in changes in the internal pressure ratio K_{av} , defined as the ratio of horizontal P_H to vertical P_V internal pressure. A higher pressure-ratio K_{av} value was observed when PSD was normal rather than skewed. Their results, however, were related to the varying shape of the PSD, rather than the PSD width and its influence on flowability.

Experimentally uniaxially compressed granular material was considered by Chung [15] and Bek et al. [5]. Both characterized the internal friction of granular materials within the cylinder, based on the measured distribution of internal pressure. The first study experimentally confirmed Janssen's theory of internal pressure transmission, whereas the second introduced the so-called granular friction analyzer (GFA) apparatus and GFA index to characterize the related flowability of uniaxially compressed granular material. Schulze [16] further showed, theoretically, that the GFA index can be related to Janssen's parameters, i.e. internal friction μ and the internal pressure ratio K . The latter, as stated in [16], makes the GFA index a potential single parameter for characterizing the flowability of granular material, rather than using Janssen's individual parameters. For this purpose, Venkatesh et al. [17] introduced an optically improved version of the GFA apparatus (O-GFA) to evaluate the GFA index of granular materials. In the same paper the relationship between the GFA index and Janssen's parameters was experimentally confirmed.

The above review of literature of granular material clearly shows the knowledge gap and lack of understanding of the influence of PSD width on the flowability of granular material under uniaxial compression loading. Therefore, this paper focuses on characterizing the influence of PSD width on the GFA index. For this purpose, samples of bronze powder with 3 different PSD widths were evaluated in experiments using the O-GFA apparatus. With this aim, the next section of the paper presents a detailed description of the GFA index and its experimental evaluation. In the third section the O-GFA experimental setup and the methodology of the experiment is described. In the fourth section, preceding the conclusions, the results of the influence of the PSD width on the GFA index are presented and discussed, together with an estimation of Janssen's parameters.

2. The GFA index and its experimental assessment

To characterize the internal friction, μ , and the related flow behavior of granular materials under compression loading, Bek et al. [5] introduced the GFA index, which is based on the realization that Newtonian fluids have the unique property of diverting the uniaxial forces acting on them uniformly in all directions. With the aim of defining the GFA index, Fig. 1 shows the distribution of the assumed hydrostatic pressure P_F in a Newtonian fluid, and the vertical internal pressure P_V of granular materials along z , the axial direction of the cylinder. As defined by Schulze

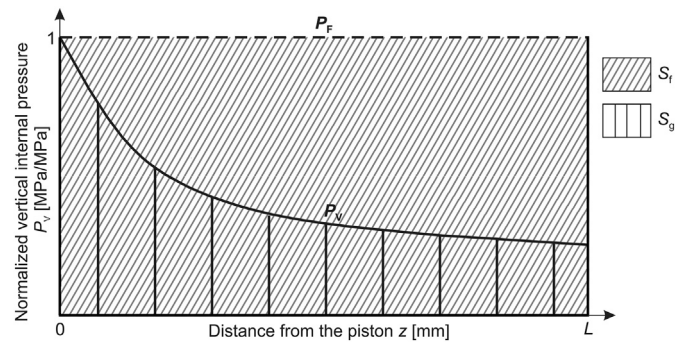


Fig. 1. Schematic presentation of Newtonian fluid $P_F(z)$ and granular material vertical pressure $P_V(z)$.

[16], the effect of gravity on the hydrostatic pressure P_F in a Newtonian fluid and on the vertical internal pressure P_V can be neglected here due to the high uniaxial compression loading compared to the weight of the powder. Due to the presence of internal friction μ , the vertical internal pressure P_V of the granular material decreases along the z -axis of the cylinder, as shown schematically in Fig. 1. On the contrary, the hydrostatic pressure P_F of Newtonian fluid is constant along the z -axis of the cylinder. Based on the pressure distribution $P_V(z)$ and $P_F(z)$ along the z -axis, the GFA index is defined by:

$$GFA_{index} = \frac{S_g}{S_f} = \frac{\int_0^L P_V(z) \cdot dz}{P_F \cdot L} = \frac{A_c \cdot \int_0^L P_V(z) \cdot dz}{F_T \cdot L}, \quad (1)$$

where S_g and S_f represent the area under the curves $P_V(z)$ and $P_F(z)$, as shown schematically in Fig. 1. In the second and third terms of Eq. (1), L is the integration length of the vertical internal pressure P_V and the hydrostatic pressure P_F along the cylinder, and A_c is the internal surface area of the cylinder. Based on Eq. (1), the GFA index values are in the interval $[0,1]$. The GFA index is equal to 1 in the case of a Newtonian fluid, while a value of less than 1 indicates the presence of internal friction μ and a decrease in flowability of granular materials. Since the vertical internal pressure P_V decreases monotonically along the length L of the cylinder, the GFA index and the related internal frictional properties of granular materials can be evaluated by analyzing the decrease in vertical internal pressure $P_V(z)$ along the length L of the cylinder. Granular material with a regressive decrease in vertical internal pressure $P_V(z)$ along the length L will have a lower GFA index and higher internal friction μ than materials with a linear or even progressive decrease in vertical internal pressure $P_V(z)$ along the z -axis of the cylinder.

With the aim of experimentally determining the GFA index and the related internal friction μ in granular materials, the thin-walled pressure-vessel elastic theory [18] was used to calculate the vertical internal pressure $P_V(z)$. Based on this theory [18], the assumed theoretical hydrostatic pressure state developed inside the cylinder, therefore the internal pressure P_F , is constant in the case of Newtonian fluid, and the corresponding strains $|\varepsilon_a|$ and ε_t , which develop on the outer surface of the cylinder, are proportional to the internal pressure P_F and constant along the z -axis, as shown in Fig. 2(a).

Furthermore, in the case of granular materials, the vertical internal pressure P_V that develops inside the material-filled cylinder of internal diameter D_i (Fig. 2(b)), and is uniaxially compressed by the force F_T , can be calculated [18] via:

$$P_V(z) = \frac{4 \cdot F_V(z)}{\pi D_i^2 \cdot (1 + \varepsilon_t)^2}. \quad (2)$$

Considering the vertical equilibrium of forces in the free-body diagram of granular materials under uniaxial compression loading F_T by a piston, schematically shown in Fig. 3, the unknown vertical force.

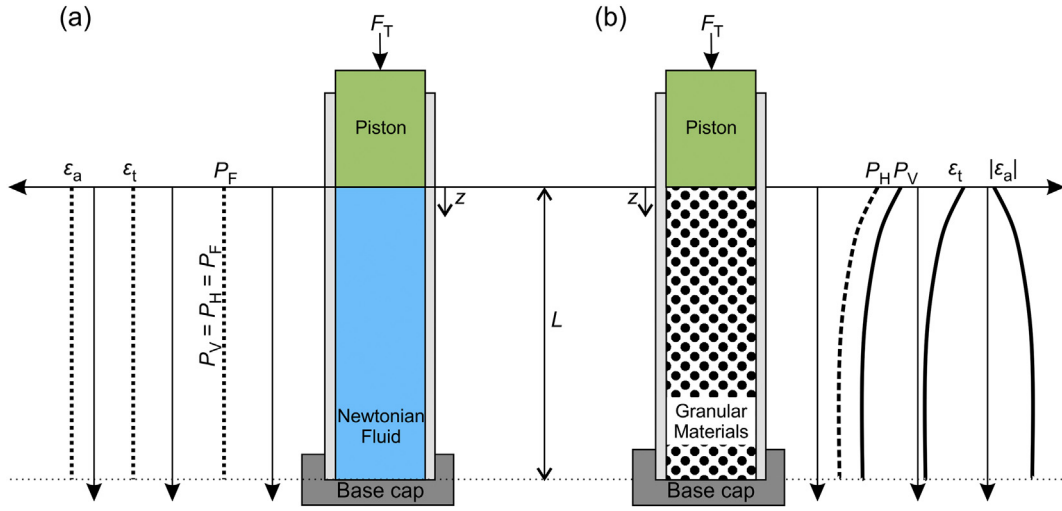


Fig. 2. Schematics of vertical $P_V(z)$ and horizontal $P_H(z)$ internal pressure; and tangential $\varepsilon_t(z)$ and absolute axial $|\varepsilon_a(z)|$ strains under uniaxial compression in the case of (a) Newtonian fluid and (b) granular materials.

F_V along the granular material in Eq. (2), is defined by:

$$F_V(z) = F_T - \pi D_i \cdot (1 + \varepsilon_t) \cdot \frac{(D_o - D_i)}{2} \cdot \sigma_a(z) \quad (3)$$

where D_o is the outer diameter of the cylinder and σ_a is the axial stress along z , the axial direction of the cylinder. The unknown axial stress σ_a in Eq. (3) can be calculated with the use of Eq. (4) as follows:

$$\sigma_a(z) = \frac{E_w(\varepsilon_a + \nu_w \cdot \varepsilon_t)}{1 - \nu_w^2} \quad (4)$$

where E_w is Young's modulus and ν_w the Poisson ratio of the cylinder material. In Eqs. (2), (3) and (4) the remaining unknown variables are the tangential and axial strains, respectively ε_t and $|\varepsilon_a|$, along the axial direction z of the cylinder wall.

Since the calculation of the GFA index is based upon confined compression of granular materials, Janssen's parameters, including the internal pressure ratio K and the internal friction μ , can also be calculated [16]. The internal pressure ratio $K(z)$ is defined as the ratio of horizontal internal pressure $P_H(z)$ to vertical internal pressure $P_V(z)$ [13]:

$$K(z) = \frac{P_H(z)}{P_V(z)}. \quad (5)$$

In order to determine $K(z)$, $P_V(z)$ can be derived from Eq. (2), and $P_H(z)$ can be calculated by:

$$P_H(z) = \frac{(D_o - D_i) \cdot \sigma_t(z)}{D_i \cdot (1 + \varepsilon_t(z))}, \quad (6)$$

where $\sigma_t(z)$ represents the tangential stress on the cylinder wall, defined by the stress-strain relationship using the measured strains:

$$\sigma_t(z) = \frac{E_w \cdot (\varepsilon_t + \nu_w \cdot \varepsilon_a)}{1 - \nu_w^2}. \quad (7)$$

In order to determine the second of Janssen's parameters, the internal friction μ , the simplified Janssen's vertical internal pressure P_V Eq. [16] can be used:

$$P_V(z) = \sigma_{v0} \cdot e^{-4 \cdot K_{av} \cdot \mu \cdot \frac{z}{D_i}}. \quad (8)$$

In Eq. (8), σ_{v0} represents the vertical stress applied on the granular materials at $z = 0$ and K_{av} denotes the average internal pressure ratio calculated from $K(z)$. Based on the experimental data for $P_V(z)$, and calculated K_{av} , the only unknown in the Eq. (8) is the internal friction μ , which is evaluated using the exponential regression method [4].

Therefore, the primary goal of a GFA apparatus is the calculation of local tangential $\varepsilon_t(z)$ and axial $|\varepsilon_a(z)|$ strains along the axial direction z of the cylinder wall which are given by [19]:

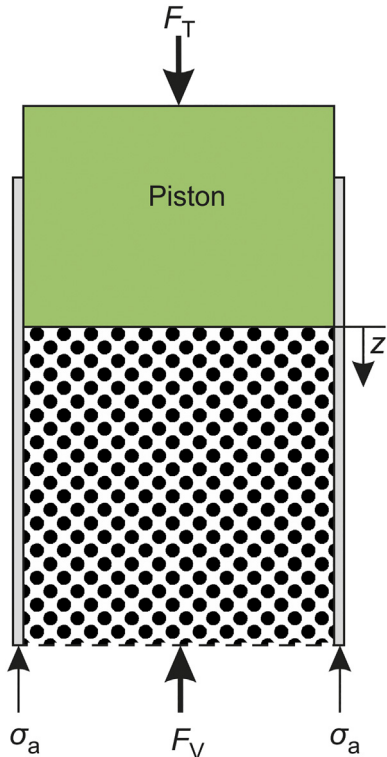


Fig. 3. Free body diagram (FBD) of granular materials filled in a cylinder and exposed to the uniaxial compression force F_T .

$$\epsilon_t(z) = \frac{\partial u}{\partial x} + \frac{1}{2} \left[\left(\frac{\partial u}{\partial x} \right)^2 + \left(\frac{\partial v}{\partial x} \right)^2 \right] \quad (9)$$

$$\epsilon_a(z) = \frac{\partial v}{\partial y} + \frac{1}{2} \left[\left(\frac{\partial u}{\partial y} \right)^2 + \left(\frac{\partial v}{\partial y} \right)^2 \right] \quad (10)$$

where, u and v are displacements along the tangential and axial direction measured by the DIC method along the axial direction z . The calculated strains $\epsilon_t(z)$ and $|\epsilon_a(z)|$ are then used to evaluate the vertical internal pressure $P_V(z)$, the related GFA index and the internal friction, μ , according to the above equations.

3. Experimental section

In the methodology presented above for evaluating the GFA index, which relies on vertical internal pressure P_V , calculated on the basis of the measured stress-strain relationship of the cylinder wall, the material properties of the alumina cylinder, including Young's modulus E_w and the Poisson ratio ν_w , are very important. For this reason, following the description of the experimental setup, results are presented from the experimental estimation of Young's modulus E_w and the Poisson ratio ν_w through uniaxial compression testing of an empty cylinder. In the last part of this section the properties of the used powder and the experiments performed are described.

3.1. Experimental setup

With the aim of experimentally measuring the GFA index and the related internal friction μ in granular materials, apparatus known as the optical granular friction analyzer (O-GFA) [17], and the above mentioned thin-walled pressure-vessel elastic theory were used. As shown schematically in Fig. 4(a), the O-GFA apparatus consists of an aluminium cylinder, a stainless-steel base cap, a stainless-steel piston for applying an uniaxial compression force F_T to granular material in the aluminium cylinder, and an optical system for measuring the deformations and related strains. The optical system consists of two LED (OSRAM LED star classic A 75 E27) illumination sources and a Point Grey USB 3.1 digital camera (5MP – GS3-U3-50S5M-C) to implement a digital image correlation (DIC) method-based measurement of the axial $|\epsilon_a(z)|$ and tangential $\epsilon_t(z)$ strains [17] on the outer surface along the z -axis of the cylinder wall, caused by uniaxially compressed granular

material inside the cylinder. The Zwick Z050 universal testing machine was used in the test arrangement to apply the uniaxial compression force F_T in a controlled manner. To prevent unbalanced deformations due to axial misalignment of the compressive axial loading a self-aligning system with bearing balls at the top end of the piston and at the bottom of the cylinder was used, as shown in Fig. 4(a). The USB 3.1 digital camera was used to capture a digital image of the cylinder wall before and after the uniaxial loading of the granular material.

For the DIC method-based measurement of strains $\epsilon_t(z)$ and $|\epsilon_a(z)|$, and the related internal vertical pressure $P_V(z)$, a DIC window of $w_s = 3$ mm width was used, consisting of 25 horizontal and 270 vertical points along the axial direction z , as indicated by the solid black line in Fig. 4(b). The captured images were analyzed with NCorr DIC software [19]. The DIC parameters used were: subset size of 25×25 pixels, spacing of 3 pixels, iteration resolution of $1e-006$, number of iterations of 50 and strain smoothing filter of size 50. The related deformations and the calculated tangential $\epsilon_t(z)$ and axial $|\epsilon_a(z)|$ strains at a given position z along the DIC window were defined as the mean value over the 25 points within the considered 3 mm width. Using the described O-GFA apparatus the vertical internal pressure P_V is measured with less than 7.5% error [17]. However, in order to avoid the edge effect at the top of the cylinder due to the piston [17], the GFA index calculation window of width $w_s = 3$ mm and height $h = 47$ mm (75×690 pixels), consisting of 25 horizontal and 230 vertical points along the axial direction z , was positioned 18 mm below the piston, as indicated by the dashed red line in Fig. 4(b). To avoid the edge effect at the bottom, and to exceed the strain resolution limit ($400 \mu\epsilon$) of the DIC setup, the bottom edge of the DIC window was positioned 90 mm above the stainless-steel base cap.

3.2. Estimation of Young's modulus and the Poisson ratio of the cylinder wall

Using the definitions of Young's modulus

$$E_w = \frac{\sigma_a}{\epsilon_a} = \frac{F_T}{\epsilon_a \cdot A_w} = \frac{4 \cdot F_T}{\epsilon_a \cdot \pi \cdot (D_o^2 - D_i^2)} \quad (11)$$

and the Poisson ratio ν_w ,

$$\nu_w = \left| -\frac{\epsilon_t}{\epsilon_a} \right|, \quad (12)$$

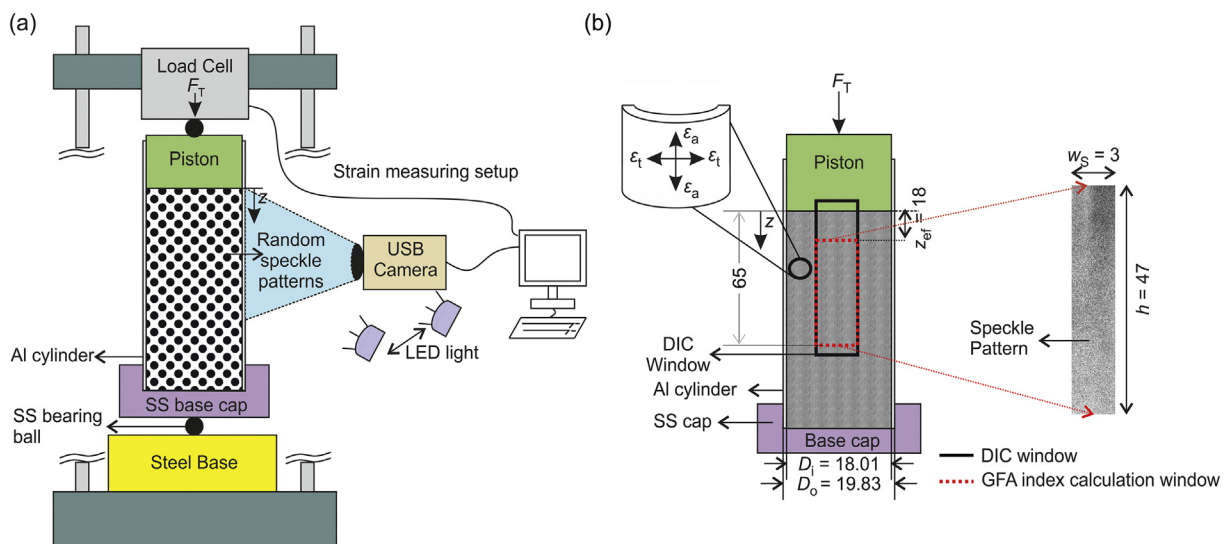


Fig. 4. Schematics of (a) O-GFA apparatus and (b) Position of the DIC and GFA index window used for strain $\epsilon_t(z)$ and $|\epsilon_a(z)|$ measurements, and calculation of vertical internal pressure P_V and the GFA index.

Young's modulus E_w and the Poisson ratio ν_w of the aluminium cylinder used can be estimated experimentally with a linear regression approach, by considering the applied uniaxial stress $\sigma_a = F_T/A_w$ and measurements of the related tangential $\varepsilon_t(z)$ and axial $|\varepsilon_a(z)|$ strains on the cylinder wall using the O-GFA apparatus described above. For this purpose, using the experimental set up shown in Fig. 4 with a piston of larger diameter, the empty aluminium cylinder was loaded 28 times at each of four predefined compression force F_T values (1510 N, 3010 N, 4510 N and 4810 N) using the Zwick universal testing machine. For each compression force F_T , the related tangential $\varepsilon_t(z)$ and axial $|\varepsilon_a(z)|$ strains of the cylinder wall were evaluated using the DIC method. To evaluate the applied uniaxial stress $\sigma_a = F_T/A_w$ at the cylinder wall, the area of the cylinder wall thickness, A_w , was estimated on the basis of the mean inner $D_i = 18.01$ mm and outer $D_o = 19.87$ mm diameters, which were calculated using 30 measurements along the cylinder circumference.

Fig. 5 shows the scatter plots $\sigma_a - |\varepsilon_a|$ and $\varepsilon_t - |\varepsilon_a|$, with strong linear regression fits in each case, yielding the respective mean estimates of the Young's modulus $\bar{E}_w = 73$ GPa and the Poisson ratio $\bar{\nu}_w = 0.42$. Taking individual measurements into account, the associated standard deviation intervals of Young's modulus and the Poisson ratio of the aluminium cylinder were defined as ± 2.2 GPa and ± 0.04 respectively.

3.3. Powder sample characteristics and experiments

To evaluate the influence of the PSD width w , on the flowability, and to characterize the internal friction μ , of granular materials, the GFA index was calculated for the three samples of bronze (CuSn 89) granular material with PSD widths of $w = 0.36, 0.87$ and 1.03 , respectively. Here the PSD width w is defined as:

$$w = \frac{D_{90} - D_{10}}{D_{50}}, \tag{13}$$

where D_{90}, D_{10} and D_{50} denote the 90th, 10th and 50th percentile of the powder sample particle size, as given in Table 1. Powders with three different PSD widths were prepared using a sieve method in accordance with the ISO standards and the associated cumulative probability functions are shown in Fig. 6 (a). Microscopic images of the granular materials in each sample were taken before the experiment and are shown in Fig. 6 (c), (d) and (e), and the related PSDs and their parameters were estimated using a digital image processing software.

Table 1
Powder sample particle size distribution parameters.

Sample i	D_{90} (μm)	D_{50} (μm)	D_{10} (μm)	m_i (μm)	σ_i (μm)	w
1	241.87	202.49	168.85	203.61	24.45	0.36
2	273.93	180.93	115.44	188.57	58.86	0.87
3	302.75	196.77	99.74	200.74	76.95	1.03

As can be seen from the powder images shown in Figs. 6 (c)-(e), the particles of granular materials were spherical. An example of the related estimates of the cumulative PSDs is shown in Fig. 6(b), which shows qualitatively good agreement with the PSDs shown in Fig. 6 (a) despite a low number of particles ($n_i = 1812, 1881$ and 1608) in the particular sample, "i", being analyzed. Based on the fact that the number of particles in the test samples used to evaluate the GFA index was much larger than n_i , due to the large size of the cylinder, it can be assumed that the PSDs and the related PSD width of the test samples used in the test performed matched well with the PSD of the supplied powder from which the test sample was taken. Furthermore the standard deviation of the mean sample particle size m_i ($\sigma_m = 7.98 \mu\text{m}$), is significantly smaller than the standard deviations σ_i of the particle size distributions of individual samples ($i = 1$ to 3), as shown in Table 1 and graphically presented in Fig. 7. Based on this, we can conclude that the variation in the mean particle size of powder samples, m_i , and its influence on the PSD width, w , is insignificant, whereas the variation in the standard deviation of powder samples, σ_i , is significant. The later was further confirmed by statistical analysis with the F-test evaluating the equality of standard deviations of samples, σ_i , yielding the highest p value of 0.0018.

For each of the three granular material samples considered, 6 repetitions of the experiment were performed. Each time the cylinder was filled with unused powder to the same level, which was ensured by checking the height of the crosshead starting position on the Zwick universal testing machine. A reference image of the speckled pattern of the filled cylinder was then taken at zero load, $F_T = 0$ N. After taking the reference image, the piston applied continuous incremental uniaxial compression loading to the granular material until a selected force of $F_T = 4810$ N was reached and an image of the speckled pattern of the deformed cylinder was recorded. The two acquired images of the speckled pattern, respectively corresponding to the undeformed and deformed cylinder, were then analyzed using the DIC method to estimate the

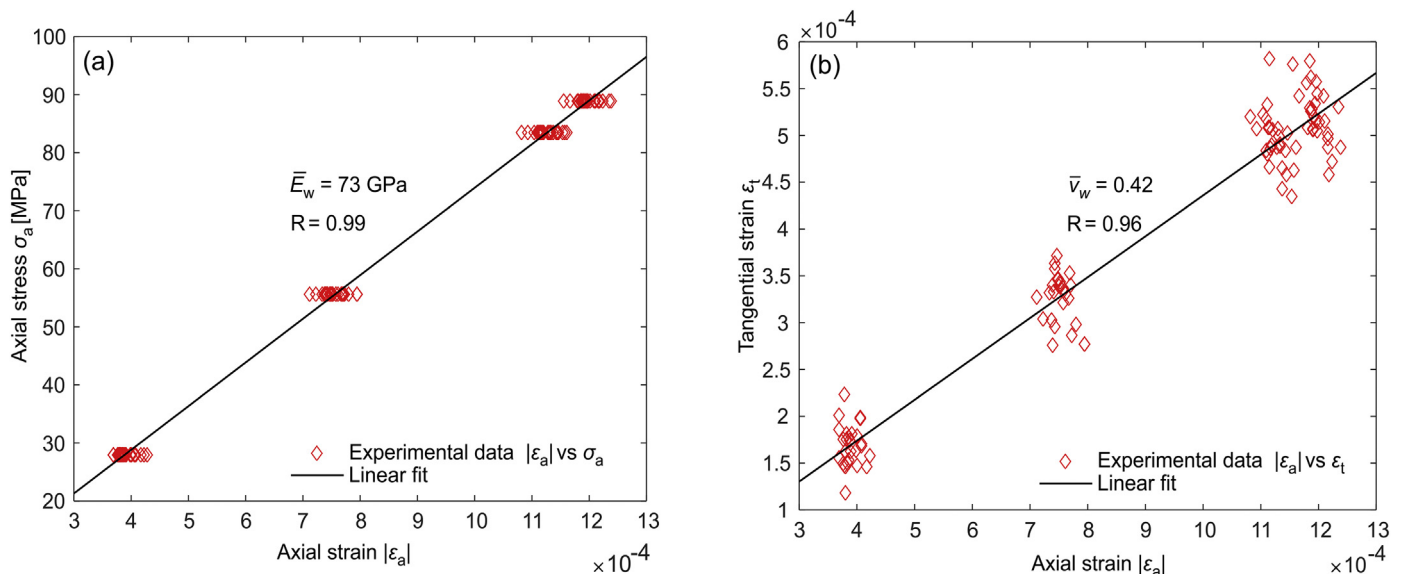


Fig. 5. Linear regression-based estimation of (a) Young's modulus E_w (b) Poisson ratio ν_w .

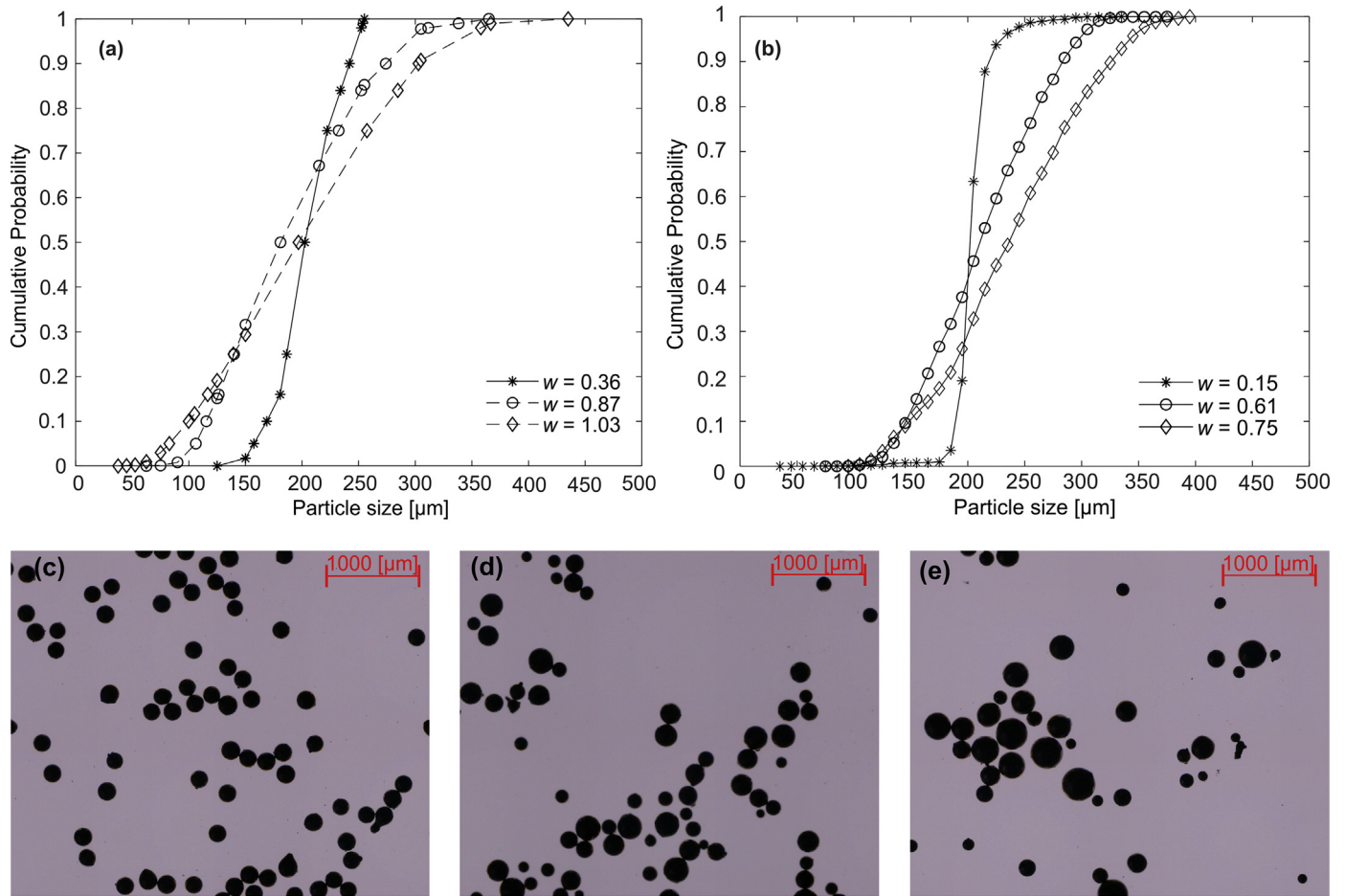


Fig. 6. (upper section): (a) cumulative probability function of the powders considered with PSD widths of $w = 0.36, 0.87,$ and $1.03,$ (b) examples of cumulative probability functions of test samples with related PSD widths of $w = 0.15, 0.61,$ and $0.75,$ (lower section): microscopic images taken before the experiment of bronze powders with different PSD widths (w) (c) $w = 0.36;$ (d) $w = 0.87,$ (e) $w = 1.03.$

tangential $\varepsilon_t(z)$ and axial $|\varepsilon_a(z)|$ strains. The latter were then used to calculate the vertical internal pressure $P_V(z)$ and the related GFA index, as described in section 2.

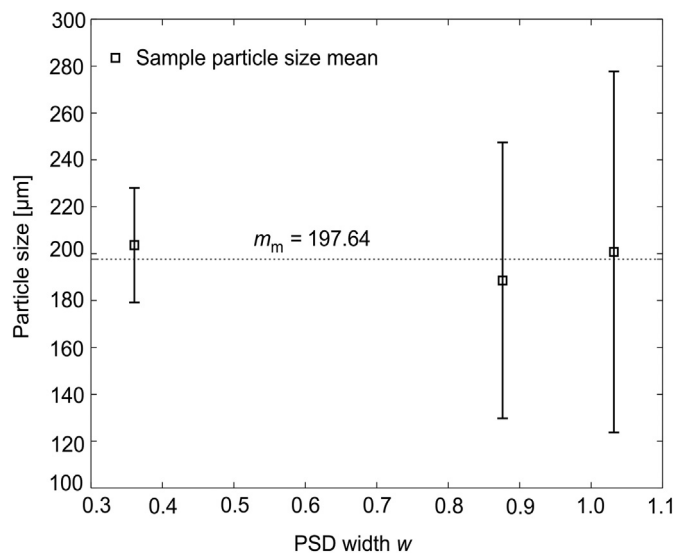


Fig. 7. Powder sample particle size grand mean value $m_m = 197.64 \mu\text{m}$ and mean values m_i of powder samples with associated standard deviation $\pm \sigma$ intervals vs. PSD width $w.$

4. Results and discussion

This section of the paper presents the results of DIC-based measurements of tangential $\varepsilon_t(z)$ and axial $|\varepsilon_a(z)|$ strains on the cylinder wall, and the related vertical $P_V(z)$ and horizontal $P_H(z)$ internal pressure along the z -axis of the cylinder. The internal pressure of the cylinder was caused by the uniaxial compression load F_T applied to the powder inside it. Furthermore, using the vertical $P_V(z)$ and horizontal $P_H(z)$ internal pressures, the results of the GFA index and Janssen's parameters as a functions of the PSD width, $w,$ are presented.

4.1. DIC method-based strain measurements

Fig. 8 shows the tangential $\varepsilon_t(z)$ and axial $|\varepsilon_a(z)|$ strains along the axial direction z of the cylinder wall, as the mean value of six measurements, for the three different PSD widths $w.$ The diagrams of $\varepsilon_t(z)$ and $|\varepsilon_a(z)|$ are shown for z -positions within the interval $[18, 67]$ mm, excluding the edge-influenced region at the top near the piston, and at the bottom of the cylinder in the vicinity of the base cap [17]. Theoretically, and as shown experimentally in Fig. 8(a), the tangential strains $\varepsilon_t(z)$ at the cylinder wall will decrease as the distance z from the piston along the axial length of the cylinder increases, due to the presence of internal friction μ when granular materials are compressed within a confined volume. On the contrary, as shown in Fig. 8(b), the absolute values of axial compressive strains $|\varepsilon_a(z)|$ at the cylinder wall increase as the distance z increases, due to the presence of internal friction $\mu.$

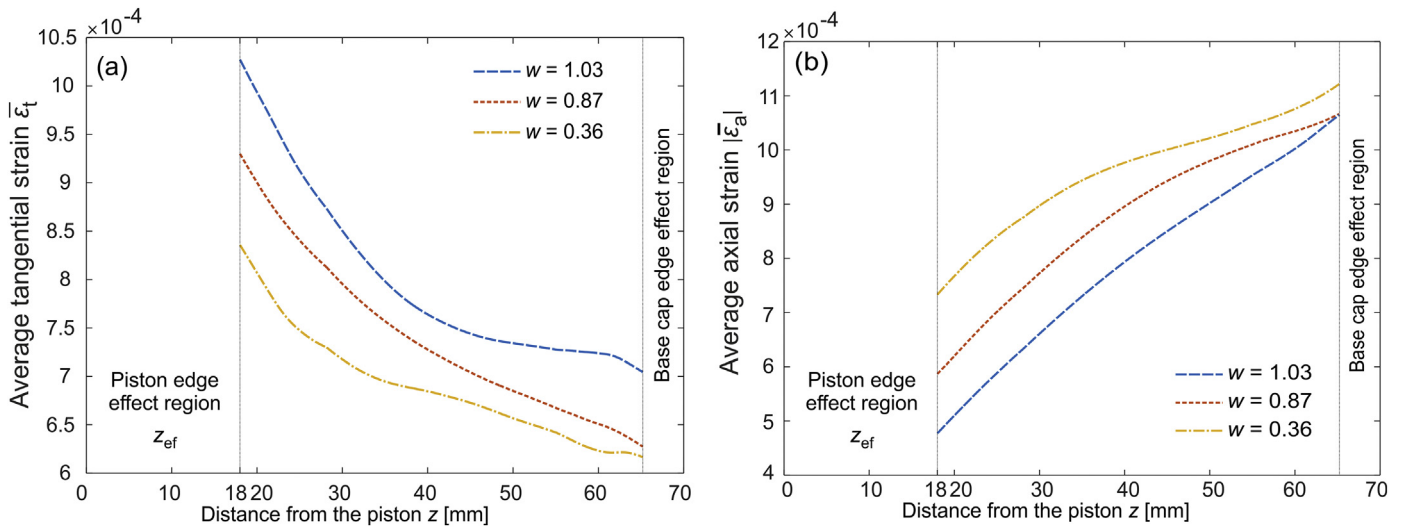


Fig. 8. Graphs of (a) mean tangential $\varepsilon_t(z)$ and (b) absolute mean axial $|\varepsilon_a(z)|$ strains vs. distance from the piston, z , for three different PSD widths $w = 0.36, 0.87$ and 1.03 .

In addition to the position z -dependent properties of the tangential $\varepsilon_t(z)$ and axial $|\varepsilon_a(z)|$ strains, Fig. 8(a) and Fig. 8(b) show that, as PSD width w increases, so does the tangential strain ε_t , whilst the compressive axial strain $|\varepsilon_a|$ decreases. Apart from the mean strains $\varepsilon_t(z)$ and $|\varepsilon_a(z)|$ shown in Fig. 8, the related set of six experimental data exhibit measurement scatter around their means, which is higher in the case of the tangential strains $\varepsilon_t(z)$. This may be related to the resolution limitation when measuring tangential strains $\varepsilon_t(z)$ using the DIC method and to the application of the 2D DIC method to a curved surface. However, based on the result of the ANOVA test on the significance of the GFA index, the difference in the curves of the mean strains $\varepsilon_t(z)$ and $|\varepsilon_a(z)|$ can be considered as statistically significant with respect to the varying values of the PSD width w , as shown in the following section 4.2.

4.2. Internal pressure and calculation of the GFA index

Based on the mean tangential $\varepsilon_t(z)$ and axial $|\varepsilon_a(z)|$ strains, the vertical $P_V(z)$ and horizontal $P_H(z)$ internal pressure along the axial direction z of the cylinder wall were calculated, according to Eqs. 2 and 6. In all cases the granular materials were loaded with an uniaxial compression load of $F_T = 4810$ N. The normalized values with respect to the applied stress of $\sigma_{v0} = 20.2$ MPa, corresponding to an uniaxial compression load of $F_T = 4810$ N, are shown in Fig. 9. As evident from the graphs in Fig. 9, the internal vertical $P_V(z)$ and horizontal $P_H(z)$ pressure, calculated from strains measured in the range $z > 18$ along the axial direction of the cylinder, decrease in a non-linear fashion, due to interparticle and particle-wall friction. It can also be observed that the vertical internal pressure $P_V(z)$ is higher than the horizontal internal pressure $P_H(z)$, and that both increase with an increase in w , the width of the sample PSD. The latter can be explained by the roller bearing effect, whereby smaller particles act as rollers between the larger particles, which results in a lower decrease in pressure throughout the granular material [13].

In accordance with the definition of the GFA index [5], the normalized vertical internal pressure $P_V(z)$ along the cylinder z -axis should be considered from the piston-powder contact at $z = 0$, at which the $P_V(z)$ has its maximal value, equal to the known applied vertical stress σ_{v0} . Therefore, the normalized vertical internal pressure P_V at $z = 0$ is equal to 1. Based on this, the normalized vertical internal pressure $P_V(z)$ values in the interval $z \in (0, 18)$ are defined by a linear extrapolation from $P_V(z = 18)$ to the normalized vertical internal pressure $P_V(z = 0) = 1$, as demonstrated in [5]. Similarly, to define the extrapolation value at the horizontal internal pressure $P_H(z = 0)$, the average internal

pressure ratio K_{av} is calculated using the 230 data points along the GFA index calculation window. The horizontal internal pressure at $P_H(z = 0)$ is then defined using the pressure ratio $P_H = K_{av} \cdot P_V(z = 0)$. Based on the defined normalized vertical internal pressure P_V , the GFA index was calculated using Eq. (1) for the samples of granular material with three different PSD widths ($w = 0.36, 0.87$ and 1.03). Based on 6 repetitions of the experiment performed at a given PSD width w , the mean value of the GFA index and the related 95% confidence intervals were calculated (see Fig. 10(a)). It can be seen that the GFA index increases with an increase in the PSD width, w . The influence of PSD width, w , on the GFA index was statistically significant, as confirmed by the ANOVA test p -value = 0.002.

Fig. 10(b) shows the mean value of the internal pressure ratio $K_{av}(z)$ from 6 trials, calculated for 230 data points along the z -direction. As mentioned by Schulze [13], and observed in Fig. 10(b), $K_{av}(z)$ does not change significantly along the z axis. The mean value of the internal pressure ratio K_{av} was therefore calculated from $K_{av}(z)$ in order to characterize it. The values of the mean internal pressure ratio K_{av} against the PSD width, w , are shown in Fig. 10(c), alongside 95% confidence intervals. It can be seen that the internal pressure ratio K_{av} increases as the

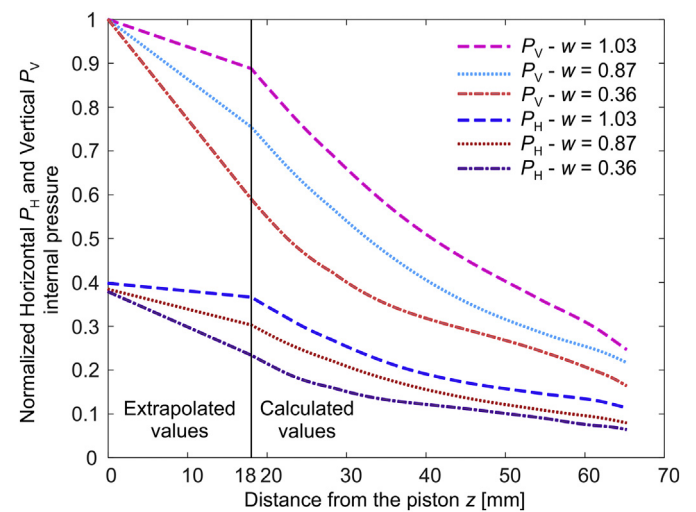


Fig. 9. Calculated normalized vertical P_V and horizontal P_H mean internal pressure with respect to the axial direction z along the considered DIC window for different PSD widths w .

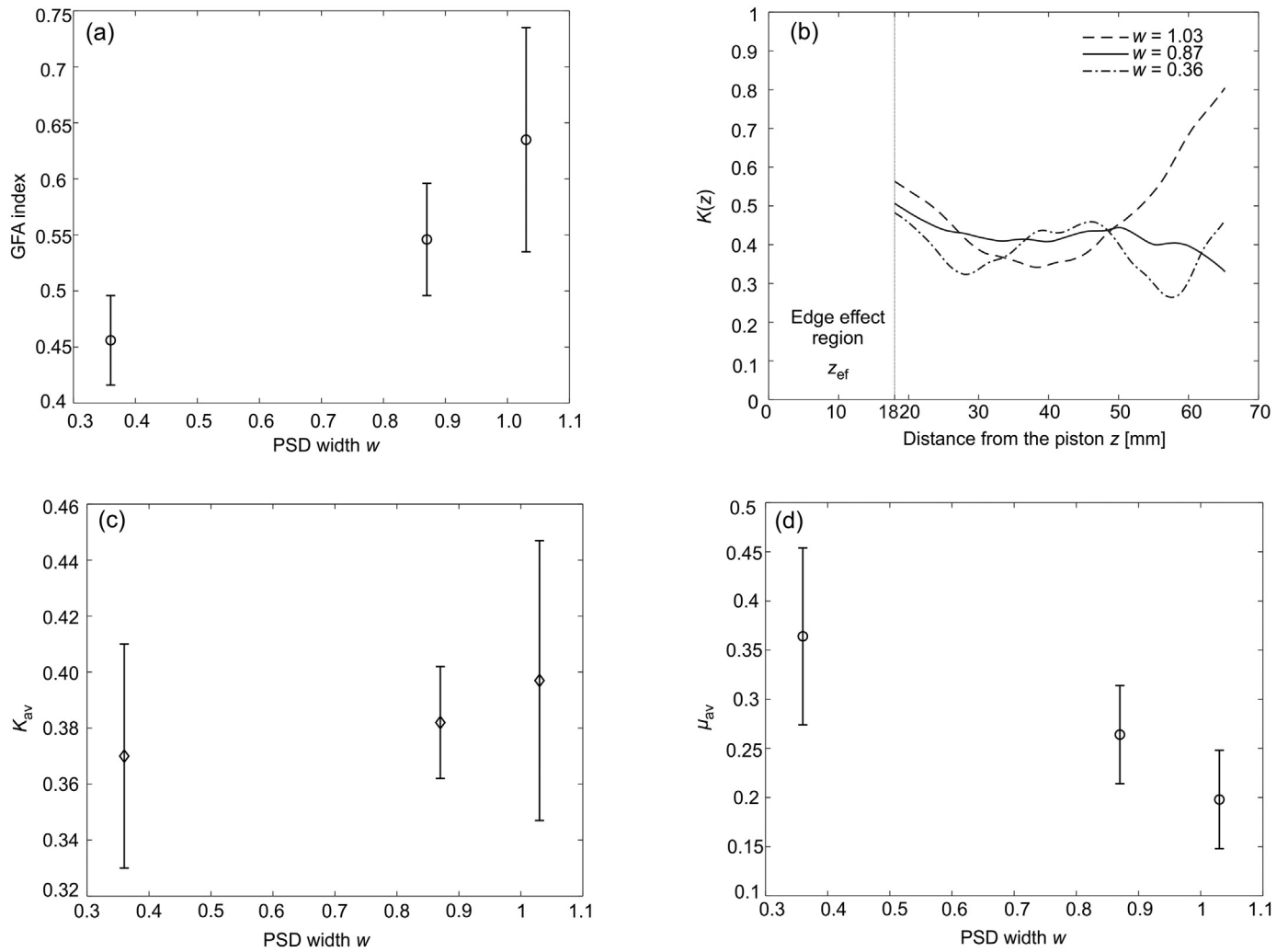


Fig. 10. (a) Mean GFA index value with 95% confidence intervals vs. PSD width w ; (b) internal pressure ratio $K(z)$ along the axial direction z of the cylinder; and Influence of PSD width, w , on the mean (c) internal pressure ratio K_{av} and (d) internal friction μ_{av} .

PSD width, w , increases. However, as evident from the graph and reported in [16], this relationship is statistically insignificant.

To evaluate the internal friction μ , the simplified Jansen's formula (Eqs. (8)) can be used. By using the experimentally evaluated vertical internal pressure $P_V(z)$ and the mean internal pressure ratio K_{av} , for each of the 6 trials of the experiment, the related internal friction μ was obtained by the regression method [4], and the related mean internal friction μ_{av} , and coefficient of determination $R^2 = 0.93, 0.96$ and 0.88 were calculated for PSD width $w = 0.36, 0.87$ and 1.03 respectively. The relationship between mean internal friction μ_{av} and PSD width w is presented in Fig. 10 (d), alongside 95% confidence intervals. It can be seen that as the PSD width, w , increases, the internal friction μ_{av} decreases. This was confirmed as statistically significant by the ANOVA test p -value = 0.005 .

The observed increase in GFA index and decrease in mean internal friction μ_{av} associated with an increase in the width of PSD, w , are related to the presence of smaller particles between the larger particles. When a certain amount of small spherical particles get between the larger particles, they induce a rolling effect, which acts as a lubricant for the large particles and improves flowability [6,7]. However, as noted in [7,20], too many small particles would increase the contact area and consequently reduce the flowability. A similar observation that granular materials with a broad PSD flow better than those with a narrow PSD has been made by Diner et al. [21].

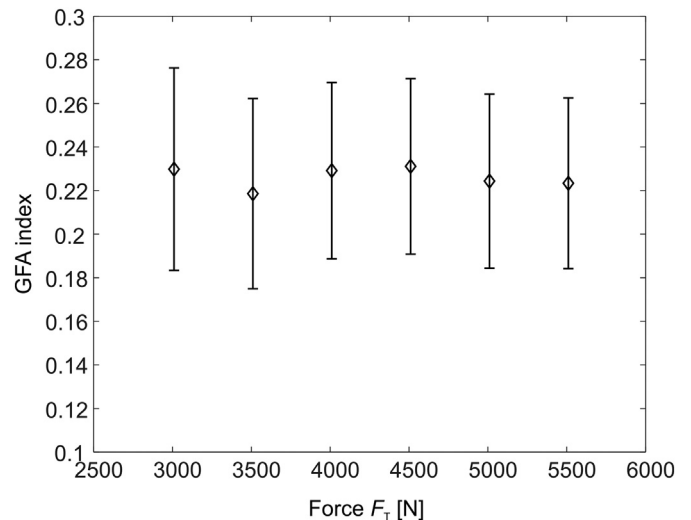


Fig. 11. Influence of the magnitude of the uniaxial force F_T on the GFA index, with 95% confidence intervals.

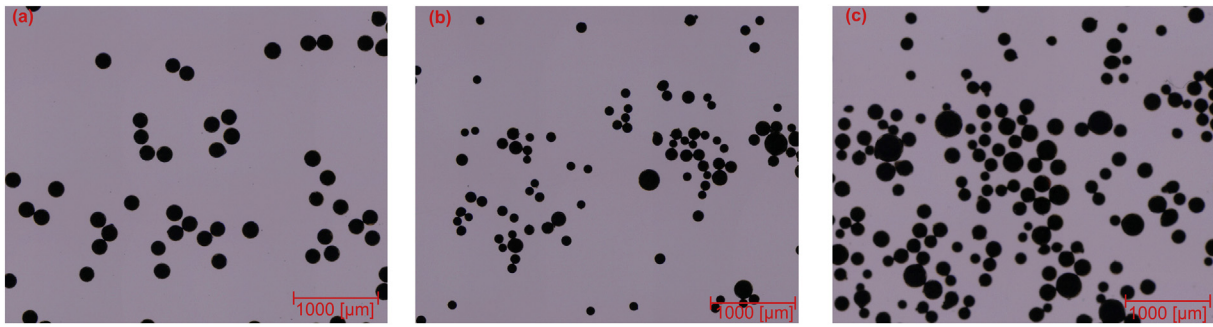


Fig. 12. Microscopic images of the 3 bronze samples of varying PSD widths, w , taken after the experiment at maximal load $F_T = 5510$ N (a) $w = 0.36$, (b) $w = 0.87$, (c) $w = 1.03$.

4.3. Discussion

The O-GFA apparatus presented, combined with the DIC method, proves to be an interesting and promising alternative method to traditional methods used for the characterization of granular materials, and the results show that the width of the PSD, w , significantly influences the GFA index. Venkatesh et al. [17] discussed the advantages of both the O-GFA apparatus and the ability to use the GFA index alone to characterize the flowability of granular material, rather than needing to use individual properties such as internal friction μ_{av} and internal pressure ratio K_{av} . They further addressed several open questions in their study, including the material and elasticity of the tube wall, the standardization of the cylinder diameter D_i , and the integration length L , which would allow better comparison and interpretation of GFA index values in the future and help establish the O-GFA apparatus as a promising tool to characterize the flowability of granular materials.

An additional open issue and potential avenue for improvement relates to the limitation of the 2D DIC method used to measure the 3D curved surface and out of plane deformations. When strains on a curved surface are measured using a 2D DIC-based method, only a very small surface can be considered in the tangential direction on the cylinder wall, in order to fulfill the required assumption of being a flat surface. In relation to this, a 3 mm width window was considered as a flat surface in the current paper. Furthermore, as reported by Venkatesh et al. [17] based on parametric error analysis, one of the major sources of error in the calculation of the GFA index comes from uncertainty of Poisson's ratio, which is primarily related to the strain measurement resolution of the O-GFA apparatus. Therefore, in order to further improve the measurement accuracy of tangential strains and the GFA index, a 3D DIC-based method of higher resolution should be used.

Another still open question, considered below, is the influence of the magnitude of the uniaxial compression force F_T on the GFA index. For this purpose, the GFA index was calculated at various loads of uniaxial compressive force F_T , namely 3010 N, 3510 N, 4010 N, 4510 N, 5010 N and 5510 N, acting on a powder with a PSD width of $w = 0.87$. For each load magnitude, 8 repetitions of the experiment were performed.

Fig. 11 shows the calculated GFA index with respect to the applied uniaxial force F_T , alongside 95% confidence intervals. From Fig. 11, and the related ANOVA test (p -value = 0.99), it can be concluded that the GFA index does not depend on the magnitude of the uniaxial compressive force, F_T , applied, within the test interval used (from 3010 N to 5510 N). However, this could not be the case if the force F_T was further increased, such that the granular material started to plasticize at the grain-level. This would alter the properties of the granular material, thus affecting its flowability and the GFA index. In order to verify the regime of grain deformation, a visual inspection of the powder was carried out by digital microscope once experimentation was complete. No significant changes in grain shape could be observed qualitatively, as shown in Fig. 12, indicating that no visible plastic deformation had occurred.

Furthermore, considering the influence of the PSD width, w , on the flowability, Schulze et al. [13] has shown that a PSD width above a certain level, i.e. with a larger number of smaller particles, would increase the internal friction μ_{av} and thus decrease the flowability, due to the cohesive nature of these particles, whereas a PSD width below this level leads to an increase in flowability. It is therefore necessary to investigate such a limit to PSD width in future work, also for uniaxial compression of granular materials under a constrained volume.

5. Conclusion

In this paper the GFA index was used to assess the influence of particle sample distribution (PSD) width, w , on the flowability of uniaxially compressed granular material. The Janssen formula was used to evaluate the internal friction μ_{av} and the internal pressure ratio K_{av} . An optical granular friction analyzer (O-GFA) and the digital image correlation (DIC) method were used to evaluate the GFA index. The DIC method is used to measure tangential and axial deformations and related strains of the cylinder caused by uniaxially compressed granular material in the cylinder. From the induced strains, the vertical $P_V(z)$ and the horizontal $P_H(z)$ internal pressure along the axial direction z of the cylinder and the related GFA index was calculated and further used to calculate the internal pressure ratio K_{av} and friction μ_{av} . Samples of bronze powders with 3 different PSD widths ($w = 0.36, 0.87, \text{ and } 1.03$) were used in the experiments to demonstrate the influence of PSD width, w , on the GFA index and the associated μ_{av} and K_{av} . The results show that as the PSD width, w , of the uniaxially compressed powder material increases, so does the GFA index, meaning that the internal friction μ_{av} decreases and the flowability of the granular material increases. The observed increase in the GFA index and the associated increase in flowability is due to the "roller bearing effect", which reduces internal friction μ_{av} (as reported in [13]). In addition, our findings indicate that the mean internal pressure ratio K_{av} does not significantly increase with an increasing width of PSD, w . This can be observed, as reported in [16], when the internal vertical $P_V(z)$ and horizontal $P_H(z)$ pressure decrease at the same rate. Further the presented results show independency of GFA index on the magnitude of the applied uniaxial compressive force, F_T , being in the elastic range of granular material what is an additional convenient property of GFA test. From the results presented regarding the GFA index and the associated internal friction μ_{av} and pressure ratio K_{av} , as well as from the results presented in [13,16], it can be concluded that the GFA index is a meaningful indicator of the flowability of uniaxially compressed granular material. The results presented show that O-GFA apparatus and the GFA index can be used as an alternative method to characterize the flowability of granular material, rather than measuring the individual properties of granular materials, i.e. the internal friction μ_{av} and pressure ratio K_{av} .

Declaration of Competing Interest

None.

Acknowledgements

The authors acknowledge the financial support of the Slovenian Research Agency (research core funding No. P2 - 0241).

Declaration of Competing Interest

The authors declare that they have no known competing financial interests or personal relationships that could have appeared to influence the work reported in this paper.

References

- [1] J. Zegzulka, D. Gelnar, L. Jezerska, A. Ramirez-Gomez, J. Necas, J. Rozbroj, Internal Friction Angle of Metal Powders, 2018 1–12, <https://doi.org/10.3390/met8040255>.
- [2] J. Horabik, M. Molenda, Mechanical Properties of Granular Materials and Their Impact on Load Distribution in Silo: A Review, 2015 <https://doi.org/10.1515/sab-2015-0001>.
- [3] J. Wiącek, P. Parafiniuk, M. Stasiak, Effect of Particle Size Ratio and Contribution of Particle Size Fractions on Micromechanics of Uniaxially Compressed Binary Sphere Mixtures, 2017 1–11, <https://doi.org/10.1007/s10035-017-0719-4>.
- [4] Y.C. Chung, C.K. Lin, P.H. Chou, S.S. Hsiau, Mechanical behaviour of a granular solid and its contacting deformable structure under uni-axial compression – part I : joint DEM – FEM modelling and experimental validation, Chem. Eng. Sci. 144 (2016) 404–420, <https://doi.org/10.1016/j.ces.2015.11.024>.
- [5] M. Bek, J. Gonzalez-Gutierrez, J.A. Moreno Lopez, D. Bregant, I. Emri, Apparatus for measuring friction inside granular materials - granular friction analyzer, Powder Technol. 288 (2016) 255–265, <https://doi.org/10.1016/j.powtec.2015.11.014>.
- [6] J. Wiącek, M. Molenda, Effect of particle size distribution on micro- and macromechanical response of granular packings under compression, Int. J. Solids Struct. 51 (2014) 4189–4195, <https://doi.org/10.1016/j.ijsolstr.2014.06.029>.
- [7] X. Xinde, Y. Shanjing, H. Ning, S. Bin, Measurement and influence factors of the Flowability of microcapsules with high-content β -carotene, Chin. J. Chem. Eng. 15 (2007) 579–585, [https://doi.org/10.1016/S1004-9541\(07\)60127-X](https://doi.org/10.1016/S1004-9541(07)60127-X).
- [8] H. Hausner, Friction conditions in a mass of metal powder, Int. J. Powder Met. 3 (1967) 7–13.
- [9] A. Jenike, Storage and flow of solids, Eng. Exp. Stat, Univ. Utah, Salt Lake City, 1961, Bull No. 123.
- [10] D. Geldart, E.C. Abdullah, A. Hassanpour, L.C. Nwoke, I. Wouters, Characterization of powder flowability using measurement of angle of repose, China Particul. 4 (2006) 104–107, [https://doi.org/10.1016/S1672-2515\(07\)60247-4](https://doi.org/10.1016/S1672-2515(07)60247-4).
- [11] H.P. Kurz, G. Münz, The influence of particle size distribution on the flow properties of limestone powders, Powder Technol. 11 (1975) 37–40, [https://doi.org/10.1016/0032-5910\(75\)80020-9](https://doi.org/10.1016/0032-5910(75)80020-9).
- [12] L.C. dos Santos, R. Condotta, M. do C. Ferreira, Flow properties of coarse and fine sugar powders, J. Food Process Eng. 41 (2018) <https://doi.org/10.1111/jfpe.12648>.
- [13] D. Schulze, Powders and Bulk Solids, Springer-Verlag, Berlin Heidelberg, 2007.
- [14] J. Wiącek, M. Molenda, Numerical analysis of compression mechanics of highly poly-disperse granular mixtures with different PSD-s, Granul. Matter 20 (2018) 1–10, <https://doi.org/10.1007/s10035-018-0788-z>.
- [15] Y.C. Chung, C.K. Lin, J. Ai, Mechanical behaviour of a granular solid and its contacting deformable structure under uni-axial compression-Part II: Multi-scale exploration of internal physical properties, Chem. Eng. Sci. 144 (2016) 421–443, <https://doi.org/10.1016/j.ces.2016.01.026>.
- [16] D. Schulze, Comment on the paper “apparatus for measuring friction inside granular materials - granular friction analyzer”, Marko Bek et al., powder Technol. 288 (2016) 255–265 [1], Powder Technol. 301 (2016) 886–888, <https://doi.org/10.1016/j.powtec.2016.07.024>.
- [17] R. Venkatesh, A. Voloshin, I. Emri, M. Brojan, E. Govekar, Digital image correlation based internal friction characterization in granular materials, Exp. Mech. 60 (2019) 481–492 [10.1007/s11340-019-00570-8](https://doi.org/10.1007/s11340-019-00570-8).
- [18] M.H. Sadd, Elasticity: Theory, Applications, and Numerics, Academic Press, 2009.
- [19] J. Blaber, B. Adair, A. Antoniou, Ncorr: open-source 2D digital image correlation Matlab software, Exp. Mech. 55 (2015) 1105–1122, <https://doi.org/10.1007/s11340-015-0009-1>.
- [20] S. Persson Ann, Flow and Compression of Granulated Powders, 2013.
- [21] D.R. Dinger, J.E. Funk, Particle-packing phenomena and their application in materials processing, MRS Bull. 22 (1997) 19–23, <https://doi.org/10.1557/S0883769400034692>.